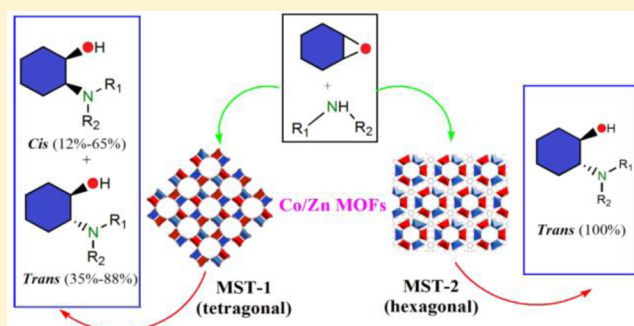


## Tetragonal versus Hexagonal: Structure-Dependent Catalytic Activity of Co/Zn Bimetallic Metal–Organic Frameworks

Anand Pariyar,<sup>†,‡</sup> Hooman Yaghoobnejad Asl,<sup>†</sup> and Amitava Choudhury<sup>\*,†</sup><sup>†</sup>Department of Chemistry, Missouri University of Science and Technology, Rolla, Missouri 65409, United States

## Supporting Information

**ABSTRACT:** Tetragonal and hexagonal phases of monometallic Zn and bimetallic Co/Zn metal–organic frameworks (MOFs), with secondary building units (SBUs) containing a  $M_3O$  ( $M = \text{metal}$ ) cluster, were synthesized from identical constituents using a benzenetricarboxylate ( $\text{BTC}^{3-}$ ) linker that forms decorated 3,6- and 3,5-connected networks, respectively. There exist subtle differences between the SBUs; one of the metal atoms in the  $M_3O$  cluster in the tetragonal phase has one dissociable DMF solvent molecule while that in the hexagonal phase has three. Connectivities between the SBUs form one-dimensional channels in both MOFs. These MOFs catalyze the chemoselective addition of amines to epoxides, giving exclusively  $\beta$ -hydroxyamine under heterogeneous conditions. A ring-opening reaction of a symmetrical epoxide showed that the hexagonal phase diastereoselectively yields *trans*-alcohol, exhibiting an exquisite model for structure-dependent activity.



## INTRODUCTION

The presence of highly ordered multidimensional cavities in crystalline porous metal–organic frameworks (MOFs) provides zeolite-like properties suitable for the design of hybrid materials with multiple functionality.<sup>1–4</sup> Precise control of the assembly of linkers and metal ions gives rise to secondary building units (SBUs) that can be designed for a targeted property, and porous structures can be constructed with these SBUs with systematic variation in pores using the concept of reticular synthesis.<sup>5</sup> Usually hydro(solvo)thermal reactions, exploiting the self-assembly of the constituents from soluble precursors under autogenous pressure, are employed to get access to those predetermined MOFs. However, under such hydro(solvo)-thermal conditions, nonequilibrium crystallization takes place and gives rise to the formation of metastable kinetic phases.<sup>6–8</sup> The main challenge here is to establish the right synthetic conditions for the synthesis of a particular type of MOF because even a subtle change in the conditions (temperature, concentration, etc.) can give rise to structures with different topologies starting from the same precursors.<sup>6</sup> Scientists have taken advantage of this fact and synthesized a plethora of MOFs with different topologies just by varying the conditions and often keeping the same constituents.<sup>9</sup> The initial applications of MOFs were focused on gas storage and separation because of the large pore volumes and tunable pore sizes.<sup>10,11</sup> However, in recent years the application of MOFs has shifted to catalysis because of the unprecedented degree of functionality arising from the coordinatively unsaturated metal sites, functional organic linkers, and tunable sizes and shapes of the pores.<sup>12,13</sup> The possibility of designing mixed-ligand/mixed-metal MOFs further adds to the tunability

capability in its catalytic attributes.<sup>14,15</sup> The porous crystalline nature of MOFs provides better precision to determine the active site within the framework.<sup>16,17</sup> Methods for the rational design of MOFs for targeted catalytic applications are also on the rise because of a better understanding of the relationship between the structure and their catalytic properties.<sup>18,19</sup> Examples of differences in the reactivity of postsynthetic modified MOFs via chemical transformation of building blocks/linkers are well demonstrated,<sup>20–24</sup> but reactivity differences of MOFs with identical/closely related building blocks are rare.<sup>25</sup> The study of such MOFs made of identical constituents, similar SBUs and structures with closely related pore geometries, for catalytic applications may lead to the formation of important models to understand the structure activity relationship in MOFs. However, it is still challenging to identify related structures to study and elucidate the structure–function relationships. In this Article, we report the synthesis and structure of two closely related MOFs formed with very similar SBUs containing a  $M_3O$  cluster and one-dimensional (1D) channels: one crystallizing in a hexagonal crystal system and the other in a tetragonal crystal system. One of the metal atoms in the  $M_3O$  cluster in the tetragonal phase has one dissociable solvent molecule, while it has three in the hexagonal phase. These solvent-bearing metal sites can act as catalytically active Lewis acid centers and thus offer a unique opportunity to test the reactivity differences of two MOFs because of subtle differences in their SBUs. We present herein the interesting differences in the stereoselectivity in epoxide ring-opening

Received: May 27, 2016

Published: September 1, 2016

Table 1. Crystal Data and Structure Refinement for MST-1(Co–Zn), MST-2(Co–Zn), and MST-2(Zn)

	MST-1(Co–Zn)	MST-2(Co–Zn)	MST-2(Zn)
empirical formula	C <sub>23</sub> H <sub>27</sub> Co <sub>0.5</sub> N <sub>2</sub> O <sub>16.5</sub> Zn <sub>2.5</sub>	C <sub>24.667</sub> H <sub>24.667</sub> Co <sub>0.5</sub> N <sub>3.333</sub> O <sub>14.667</sub> Zn <sub>2.5</sub>	C <sub>24.667</sub> H <sub>24.667</sub> N <sub>3.333</sub> O <sub>14.667</sub> Zn <sub>3</sub>
fw	788.36	801.42	804.64
temperature (K)	298(2)	230(2)	220(2)
wavelength (Å)	0.71073	0.71073	0.71073
cryst syst	tetragonal	hexagonal	hexagonal
space group	I4cm	P6 <sub>3</sub> cm	P6 <sub>3</sub> cm
unit cell dimens			
<i>a</i> (Å)	20.328(9)	18.389(5)	18.368(10)
<i>b</i> (Å)	20.328(9)	18.389(5)	18.368(10)
<i>c</i> (Å)	17.910(8)	17.969(5)	17.964(10)
α (deg)	90	90	90
β (deg)	90	90	90
γ (deg)	90	120	120
volume (Å <sup>3</sup> )	7401(7)	5262(3)	5249(6)
Z	8	6	6
density (calcd) (Mg/m <sup>3</sup> )	1.415	1.517	1.529
abs coeff (mm <sup>-1</sup> )	1.813	1.995	2.105
F(000)	3196	2447	2456
θ range for data collection (deg)	1.417–28.280	2.215–28.309	2.218–28.397
index ranges	–26 ≤ <i>h</i> ≤ 26, –26 ≤ <i>k</i> ≤ 26, –23 ≤ <i>l</i> ≤ 23	–22 ≤ <i>h</i> ≤ 22, –22 ≤ <i>k</i> ≤ 22, –22 ≤ <i>l</i> ≤ 22	–24 ≤ <i>h</i> ≤ 24, –23 ≤ <i>k</i> ≤ 24, –21 ≤ <i>l</i> ≤ 23
reflins collected	47055	52636	31394
indep reflins	4706 [R(int) = 0.1119]	3648 [R(int) = 0.0824]	4462 [R(int) = 0.0886]
completeness to θ (%)	99.9	99.9	99.5
data/restraints/param	4706/199/227	3648/210/228	4462/171/221
GOF on F <sup>2</sup>	1.079	1.157	1.050
final R indices [ <i>I</i> > 2σ( <i>I</i> )]	R1 = 0.0637, wR2 = 0.1576	R1 = 0.0890, wR2 = 0.2113	R1 = 0.0530, wR2 = 0.1255
R indices (all data)	R1 = 0.0880, wR2 = 0.1769	R1 = 0.0940, wR2 = 0.2138	R1 = 0.0841, wR2 = 0.1425
absolute structure param	0.02(3)	0.00(8)	0.00(2)
δF (e/Å <sup>3</sup> )	+1.53 and –0.788	+0.906 and –2.269	+0.659 and –0.411

catalysis, demonstrating strong evidence of structure-dependent catalysis in MOFs.

## EXPERIMENTAL SECTION

**Materials and Physical Measurements.** Cobalt nitrate [Co(NO<sub>3</sub>)<sub>2</sub>·6H<sub>2</sub>O] and zinc nitrate [Zn(NO<sub>3</sub>)<sub>2</sub>·6H<sub>2</sub>O] were purchased from Alfa Aesar. 1,3,5-Benzenetricarboxylic acid (H<sub>3</sub>BTC), pyrazine, and *N,N'*-dimethylformamide (DMF) were purchased from Sigma-Aldrich. All substrates (amines and epoxides) for catalytic reactions were used as received unless otherwise mentioned. Single-crystal X-ray diffraction (SCXRD) intensity data sets were collected on a Bruker Smart Apex diffractometer with monochromated Mo Kα radiation (0.7107 Å). Powder X-ray diffraction (PXRD) was performed with finely ground powders using a PANalytical X'Pert Pro diffractometer equipped with a Cu Kα<sub>1,2</sub> anode and a linear-array PIXcel detector over a 2θ range of 5–90° with an average scanning rate of 0.0472°/s. CHN elemental analysis was conducted with a PerkinElmer model 2400 CHN elemental analyzer, calibrated with acetanilide purchased from the National Bureau of Standards. Thermogravimetric analysis (TGA) of the samples was performed with a TA Instruments Q50 thermogravimetric analyzer with a scan rate of 10 °C/min under a N<sub>2</sub> flow rate of 40 mL/min. Fourier transform infrared (FT-IR) spectra were collected using a Thermo Nicolet Nexus 470 FT-IR spectrometer over 400–4000 cm<sup>-1</sup> on a sample embedded in KBr pellets. Diffuse-reflectance spectra (DRS) were collected using Labsphere integrating sphere (model RSA HP 8453) fitted on a Varian CARY 100 Bio UV–vis spectrophotometer. DRS data were converted to absorption using a Kubelka–Munk function.<sup>26</sup> <sup>1</sup>H and <sup>13</sup>C NMR experiments were performed on a 400 MHz Bruker NMR instrument. N<sub>2</sub> gas adsorption and desorption experiments were performed using a Quantachrome

Autosorb-1 instrument at 77 K. Prior to experiments, the well-ground as-prepared samples were outgassed at 120 °C under vacuum for 12 h.

**Synthesis.** For all of the syntheses, a homogeneous solution of appropriate molar ratios of metal salt, pyrazine, and 1,3-BTC in DMF was sealed in either a glass or a polypropylene bottle. The sealed bottle was kept in a 100 °C preheated oven for 48 h for solvothermal reaction to grow crystals. After the reaction, the mother liquor was removed via pipette and replenished with fresh DMF, to ensure complete removal of the mother liquor. The crystals were filtered using vacuum filtration and washed with DMF followed by acetone. The reactions are schematically shown in the experimental section of the Supporting Information, section I.1.

**Synthesis of [Zn<sub>2.5</sub>Co<sub>0.5</sub>(μ-O)(BTC)<sub>2</sub>(DMF)(H<sub>2</sub>O)<sub>1.5</sub>(H<sub>3</sub>O)((CH<sub>3</sub>)<sub>2</sub>NH<sub>2</sub>)]<sub>n</sub>, MST-1(Co–Zn).** To a 8 mL solution of Zn(NO<sub>3</sub>)<sub>2</sub>·6H<sub>2</sub>O (0.134 g, 0.45 mmol) in DMF was added Co(NO<sub>3</sub>)<sub>2</sub>·6H<sub>2</sub>O (0.0146 g, 0.05 mmol), and the resulting solution was stirred until completely dissolved. To this clear pink solution were added H<sub>3</sub>BTC (0.105 g, 0.5 mmol) and pyrazine (0.0202 g, 0.25 mmol), and the resulting solution was stirred vigorously until completely dissolved. After solvothermal reaction, pink crystals were obtained. Yield: 0.126 g. Crystal data: *a* = *b* = 20.328(9) Å, *c* = 17.910(8) Å, α = β = γ = 90°; tetragonal; space group I4cm (No. 108). FT-IR (KBr, cm<sup>-1</sup>): 719, 761, 1110, 1373, 1440, 1567, 1625, 3414.

**Synthesis of [Zn<sub>2.5</sub>Co<sub>0.5</sub>(μ-O)(BTC)<sub>5/3</sub>(DMF)<sub>3</sub>((CH<sub>3</sub>)<sub>2</sub>NH<sub>2</sub>)<sub>0.33</sub>(H<sub>3</sub>O)<sub>0.667</sub>]<sub>n</sub>, MST-2(Co–Zn).** To a 10 mL solution of Zn(NO<sub>3</sub>)<sub>2</sub>·6H<sub>2</sub>O (0.669 g, 2.25 mmol) in DMF was added Co(NO<sub>3</sub>)<sub>2</sub>·6H<sub>2</sub>O (0.073 g, 0.25 mmol), and the resulting solution was stirred until completely dissolved. To this clear pink solution were added H<sub>3</sub>BTC (0.525 g, 2.5 mmol) and pyrazine (0.101 g, 1.25 mmol), and the resulting solution was stirred vigorously until completely dissolved. Pink crystals were obtained after solvothermal reaction. Yield: 0.718 g. Crystal data: *a* = *b* = 18.389(5) Å, *c* = 17.969(5) Å, β = 120°;

hexagonal; space group  $P6_3cm$  (No. 185). FT-IR (KBr,  $\text{cm}^{-1}$ ): 719, 761, 1108, 1375, 1442, 1573, 1625, 3417.

**Synthesis of  $[\text{Zn}_3(\mu\text{-O})(\text{BTC})_2(\text{DMF})(\text{H}_2\text{O})_{1.5}(\text{H}_3\text{O})((\text{CH}_3)_2\text{NH}_2)]$ , MST-1(Zn).** To a 8 mL solution of  $\text{Zn}(\text{NO}_3)_2 \cdot 6\text{H}_2\text{O}$  (0.149 g, 0.5 mmol) in DMF were added  $\text{H}_3\text{BTC}$  (0.105 g, 0.5 mmol) and pyrazine (0.0202 g, 0.25 mmol), and the resulting solution was stirred vigorously until completely dissolved. Solvothermal reaction yielded a colorless microcrystalline product. A good single crystal could not be obtained, and the product was characterized by PXRD, which matched very well with the simulated pattern of MST-1(Co–Zn). Yield: 0.142 g. FT-IR (KBr,  $\text{cm}^{-1}$ ): 719, 762, 1109, 1378, 1443, 1570, 1625, 3417.

**Synthesis of  $[\text{Zn}_3(\mu\text{-O})(\text{BTC})_{5/3}(\text{DMF})_3((\text{CH}_3)_2\text{NH}_2)_{0.33}(\text{H}_3\text{O})_{0.667}]$ , MST-2(Zn).** To a 10 mL solution of  $\text{Zn}(\text{NO}_3)_2 \cdot 6\text{H}_2\text{O}$  (0.743 g, 2.5 mmol) in DMF were added  $\text{H}_3\text{BTC}$  (0.525 g, 2.5 mmol) and pyrazine (0.101 g, 1.25 mmol), and the resulting solution was stirred vigorously until completely dissolved. Solvothermal reaction resulted in pure colorless crystals. Yield: 0.690 g. Crystal data:  $a = b = 18.368(10)$  Å,  $c = 17.964(10)$  Å,  $\beta = 120^\circ$ ; hexagonal; space group  $P6_3cm$  (No. 185). FT-IR (KBr,  $\text{cm}^{-1}$ ): 719, 758, 1112, 1373, 1444, 1573, 1625, 3419.

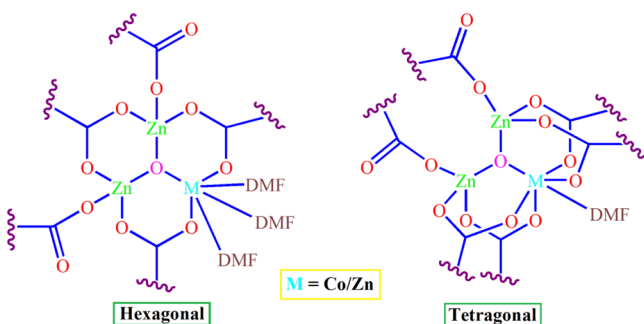
**Catalytic Epoxide Ring Opening with Amine.** In a typical reaction, 50 mg of catalyst was added to a 4 mL screw-capped vial containing small magnetic beads. To this was added 1 mmol of amine, followed by 1 mmol of epoxide. The reaction was then kept in a magnetic stirrer at  $40^\circ\text{C}$  for 12 h. After the requisite time, an aliquot was withdrawn from the reaction mixture, and the product was determined using  $^1\text{H}$  NMR by dissolving in  $\text{CDCl}_3$ . The product was isolated using literature methods and characterized by NMR and IR.

**Crystal Structure Analysis.** Suitable crystals of hexagonal and tetragonal phases were selected and mounted on a glass fiber using epoxy-based glue. The data were collected at 220 K and room temperature employing a scan of  $0.3^\circ$  in  $\omega$  with an exposure time of 20 s/frame. The data sets were collected using SMART software,<sup>27</sup> the cell refinement and data reduction were carried out with SAINT,<sup>28</sup> and the program SADABS<sup>28</sup> was used for absorption correction. The structures were solved by direct methods using SHELX-97 and difference Fourier syntheses.<sup>29</sup> Full-matrix least-squares refinement against  $|F^2|$  was carried out using the SHELXTL suite.<sup>29</sup> It is to be noted here that all of the single-crystal structures reported herein have severe disorder of the charge-balancing organoammonium cations residing in the channels. They were modeled based on the information from elemental analysis and spectroscopy. For the final refinement, the ratio of Co and Zn in the same crystallographic site was fixed based on the data obtained from spectroscopic analysis. Details of the refinement and structural parameters are given in Table 1.

## RESULTS AND DISCUSSION

**Synthesis and Crystal Structure.** We initiated the study by designing a new  $\text{M}_3\text{O}$  ( $\text{M} = \text{metal}$ ) cluster containing Co/Zn bimetallic tetragonal MST-1(Co–Zn) (MST = Missouri University of Science and Technology) and hexagonal MST-2(Co–Zn) MOFs using  $\text{H}_3\text{BTC}$  (Scheme 1). The Co/Zn

**Scheme 1.**  $\text{M}_3\text{O}$  Clusters Found in MOFs MST-2 and MST-1, Respectively



bimetallic MOFs were formed by the reaction of mixed-metal salts,  $\text{Co}(\text{NO}_3)_2 \cdot 6\text{H}_2\text{O}$ , and  $\text{Zn}(\text{NO}_3)_2 \cdot 6\text{H}_2\text{O}$  with  $\text{H}_3\text{BTC}$  and pyrazine in DMF at  $100^\circ\text{C}$ . Variation of the concentration of the reactants resulted in tetragonal (MST-1) and hexagonal (MST-2) phases (see the Experimental Section for details) as crystalline pink products. The two phases were formed with excellent bulk purity, as seen through a comparison of the simulated and experimental PXRD patterns of the bulk samples (Figures S1 and S2). SCXRD studies showed that both structures are based on a trinuclear  $\text{M}_3\text{O}$  cluster with a  $\text{MO}_6$  octahedron ( $\text{M} = \text{Co/Zn}$ ) and two  $\text{ZnO}_4$  tetrahedra corner-sharing a  $\mu_3\text{-O}$  species (Figure 1). The framework of MST-1

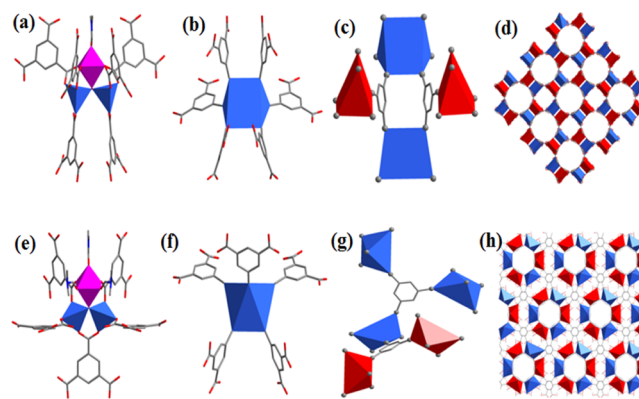


**Figure 1.** Structures of MST-1 (a–d) and MST-2 (e–h) MOFs showing coordination of  $\text{BTC}^{3-}$  to form a  $\text{M}_3\text{O}$  cluster consisting of Zn/Co $\text{O}_6$  octahedra (pink) and  $\text{ZnO}_4$  tetrahedra (blue) shared by a  $\mu_3\text{-O}$  atom in (a) MST-1 and (e) MST-2. The formation of (b) a trigonal-prismatic SBU for the MST-1 phase and (f) a trapezoidal-pyramidal SBU for the MST-2 phase with carboxylate C atoms at the vertices. (c) Decorated 3,6-connected network for MST-1 and (g) decorated 3,5-connected network for MST-2. (d and h) Perspective 3D view of the packing diagram along the  $c$  axis. The red/blue-colored SBUs represent identical units from different planes.

was found to be isostructural to previously reported  $\text{Zn}_3\text{O}$  clusters containing MOFs with  $\text{BTC}^{3-}$  such as MOF-38,<sup>30</sup> NTU-Z11,<sup>31</sup> and MOF-CJ3;<sup>32</sup> however, there exist subtle differences in the compositions and coordination environments of the metals (vide infra). The corresponding analogous monometallic tetragonal MST-1(Zn) was also obtained similarly under the same reaction conditions, as is evident from the PXRD pattern (Figure S3). On the other hand, no structural congener for MST-2 and its colorless crystalline isostructural monometallic counterpart MST-2(Zn) (Figure S4) was found in the literature. The respective Co contents in MST-1(Co–Zn) and MST-2(Co–Zn) were quantified by atomic absorption spectroscopy and corroborated by magnetic susceptibility measurements (Figure S5). The magnetic susceptibility measured between 2 and 300 K shows paramagnetic high-spin  $\text{Co}^{\text{II}}$   $d^7$  species with effective magnetic moments  $\mu_{\text{eff}} = 4.1$  and  $3.98 \mu_{\text{B}}$ , respectively, for MST-1(Co–Zn) and MST-2(Co–Zn) (Figure S5). The pink color in Co-doped MST-1(Co–Zn) and MST-2(Co–Zn) is exhibited as a result of the  $\text{Co}^{2+}$  ion occupying the octahedral site (analogous to Co–Zn/MOF-4)<sup>33</sup> in both the hexagonal and tetragonal phases. The presence of  $\text{Co}^{2+}$  in the tetrahedral site otherwise would have resulted in a blue color.<sup>33</sup> The spectra show a broad absorption peak in the visible region between 600 and 450 nm (Figure S6), indicative of octahedral  $\text{Co}^{\text{II}}$  absorption,<sup>34</sup> while the relative literature value for absorption due to tetrahedral



Co<sup>II</sup> is at lower energy between 590 and 650 nm with an intense feature due to the removal of the center of symmetry in  $T_d$  geometry.<sup>34</sup> Using the octahedral symmetry, the peak at 530 nm (18867 cm<sup>-1</sup>) can be assigned to  ${}^4T_{1g}(F) \rightarrow {}^4T_{1g}(P)$  and the shoulder at 480 nm (20833 cm<sup>-1</sup>) to  ${}^4T_{1g}(F) \rightarrow {}^4A_{2g}(F)$  transitions, respectively.<sup>35</sup>

In **MST-1** phases, each of the two crystallographically identical tetrahedral Zn<sup>2+</sup> centers is bound by two bridging bidentate and one monodentate carboxylates, while the octahedral Co/Zn site is bound by a total of four bridging bidentate carboxylates and a terminal DMF (Figure 1a). Thus, the M<sub>3</sub>O cluster is made up of a corner-sharing of two ZnO<sub>4</sub> tetrahedra and one Co/ZnO<sub>6</sub> octahedron through a common O atom,  $\mu_3$ -O(7). In contrast to **MST-1**, the two crystallographically identical Zn sites of the Zn<sub>3</sub>O cluster in **MOF-38**,<sup>30</sup> **MOF-CJ3**,<sup>32</sup> and **NTU-Z11**,<sup>31</sup> contain trigonal-bipyramidal coordination because of an additional H<sub>2</sub>O bound to the ZnO<sub>4</sub>(carboxylate) tetrahedra. In **NTU-Z11**, the sixth coordination of the octahedral moiety of the Zn<sub>3</sub>O cluster is replaced by coordinated H<sub>2</sub>O because the synthesis did not employ any DMF. Important differences also exist in the charge-balancing cations; for example, the charge of the anionic framework of **MOF-38**<sup>30</sup> is balanced by triethylammonium cations. For **MOF-CJ3**,<sup>32</sup> one hydronium balances the charge because the  $\mu_3$ -O atom was protonated, and for **NTU-Z11**,<sup>31</sup> two coordinated H<sub>2</sub>O molecules were protonated to balance the charge, which was rather unusual. In our case, **MST-1** phases contain one dimethylammonium ion and one hydronium ion (the decomposition product of DMF and protonated H<sub>2</sub>O, respectively) as charge-balancing cations, while **MST-2** also contains dimethylammonium and hydronium as counterions but in a different ratio. This is supported by elemental analysis and TGA, FT-IR signatures, and <sup>1</sup>H NMR spectra. The FT-IR spectra of the samples recorded (Figure S7) along with DMF and dimethylammonium chloride (DMACl) show characteristic NH<sub>2</sub> vibration bands at 3427 cm<sup>-1</sup> [ $\nu$ (NH<sub>2</sub>) stretching], 1581 cm<sup>-1</sup> [ $\nu$ (NH<sub>2</sub><sup>+</sup>) bending], and 1462 cm<sup>-1</sup> [ $\nu$ (NH<sub>2</sub><sup>+</sup>) bending] along with bands at 2929 and 2852 cm<sup>-1</sup> for DMF and at 1620 cm<sup>-1</sup> for  $\nu$ (C=O) (Figure S7). Furthermore, the <sup>1</sup>H NMR spectra of the leached MOFs in D<sub>2</sub>SO<sub>4</sub> show resonance peak at  $\delta = -3.46$  ppm, characteristic of the dimethylammonium cation referenced by collecting a blank spectrum of DMACl in D<sub>2</sub>SO<sub>4</sub> (Figure S8).

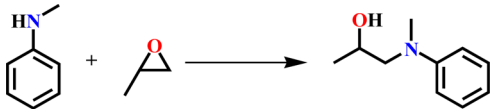
In **MST-2**, the octahedral Co<sup>2+</sup>/Zn<sup>2+</sup> center contains three terminal DMF and two bidentate carboxylates bridging the two Zn<sup>2+</sup> centers, while each of the two tetrahedral Zn<sup>2+</sup> centers is bound by one monodentate carboxylate and two bidentate carboxylates, bridging the Zn<sup>2+</sup>/Co<sup>2+</sup> and Zn<sup>2+</sup> centers in the M<sub>3</sub>O cluster formed through  $\mu_3$ -O (Figure 1e). The four equatorial Co/Zn–O(carboxylate) bond distances in **MST-1** ranging between 2.074(7) and 2.094(6) Å are comparable to each other and slightly lower than that found in **MST-2** [2.102(1) Å]. The axial Co/Zn–O bond length for coordinated DMF molecules is 2.089(6) Å, and the corresponding *trans*-Co/Zn– $\mu_3$ -O bond length is 2.115(2) Å. The Co/Zn– $\mu_3$ -O bond distance in **MST-2** was found to be 2.098(6) Å, which is slightly lower than that in **MST-1**. In **MST-2**(Co–Zn), the pure Zn– $\mu_3$ -O bond distance [1.965(2) Å] falls in the intermediate range compared to the Zn–O(carboxylate) distances that range between 1.927(2) and 1.975(9) Å. The Co/Zn–O(DMF) bond lengths are in the range 2.043(9)–2.063(9) Å.

Elaborating on the topology of the structures, six different carboxylate C atoms form the vertices of a trigonal-prismatic SBU (Figure 1b), which gives rise to a 3,6-connected network (Figure 1c) for **MST-1** similar to that known for **MOF-38**.<sup>30</sup> Each of these trigonal-prismatic inorganic SBUs links to six triangular BTC units, and each BTC unit links to three SBUs throughout the structure, as shown in Figure 1d. Such connectivities between the SBUs lead to the formation of two types of 1D channels along the *c* axis, one with smaller (square) dimensions of 6.08 × 6.08 Å, filled with hydronium cations, and the other channel with bigger dimensions of 10.53 × 10.53 Å, which hosts the charge-balancing dimethylammonium cations. It is to be noted here that the bigger dimension channels of both **MOF-CJ3**<sup>32</sup> and **NTU-Z11**<sup>31</sup> have been reported to be empty. In **MST-2**, five carboxylate C atoms attached to the M<sub>3</sub>O cluster come together to occupy the corners of a trapezoidal-pyramidal SBU (Figure 1f), which gives rise to a 3,5-connected coordination network (Figure 1g) to form a three-dimensional (3D) framework and subsequently forms one type of 1D channel along the *c* axis with dimensions of 11.51 × 11.51 Å, filled with organoammonium and hydronium ions. The N<sub>2</sub> sorption analysis at 77 K showed very low uptake (Figure S9), and Brunauer–Emmett–Teller surface area calculations revealed surface areas of 12.5 and 6.5 m<sup>2</sup>/g respectively for **MST-1**(Co–Zn) and **MST-2**(Co–Zn). Surface area measurements confirm that the micropores are inaccessible and support the presence of cations in the channels.

**Catalytic Studies.** It is to be noted that the syntheses of the MOFs reported herein are identical in terms of the relative molar ratios of the reactants. The only difference is the absolute concentration of the reactants, which is 5 times higher for the hexagonal phases, **MST-2**, compared to the tetragonal phases, **MST-1**. Their SBUs, although not identical, are quite similar. In addition to the presence of very similar SBUs and pore structures, the presence of coordinated DMF molecules (one in the tetragonal phase and three in the hexagonal phase) should play a crucial role in generating coordinatively unsaturated sites (CUSs) for interaction with the substrates. However, the removal of DMF to create CUSs under mild thermal treatment was not successful. On the other hand, heating the samples at 150 °C under vacuum turned the color of **MST-1**(Co–Zn) and **MST-2**(Co–Zn) from pink to blue (Figure S10) because of a change in the Co<sup>2+</sup> coordination corroborating with the loss of DMF, as verified by TGA (Figures S11 and S12). However, this process was also accompanied by a substantial loss of the crystallinity of the solids (Figure S13). Realizing that these coordinated DMF molecules can undergo exchange with other O donors in solution, we explored this opportunity and performed a systematic study toward evaluating the catalytic property of the phases. We choose the N–C bond-forming epoxide ring-opening (ERO) reaction with amines that yields  $\beta$ -hydroxyamine, known to be an important building motif for drugs and pharmaceuticals, as a model organic reaction to study the catalytic properties.<sup>36,37</sup> One of the direct methods for the synthesis of  $\beta$ -aminoalcohols is the direct aminolysis of epoxide. A large number of catalysts facilitate this reaction; these include the use of silica,<sup>38</sup> alumina,<sup>39</sup> alkali-metal perchlorates and tetrafluoroborates,<sup>40</sup> metal triflates,<sup>41,42</sup> metal alkoxides,<sup>43</sup> metal halides,<sup>44–47</sup> organocatalysts,<sup>48</sup> etc., to name a few. Among several catalysts, the ERO reaction, catalyzed by Schiff base containing metal complexes, is extensively studied by Jacobsen and forms the background for a mechanistic understanding of asymmetric ERO reactions.<sup>37</sup> The activation of epoxide by a

metal center, followed by nucleophilic attack by amines, alcohols, or azides to form stereoselective products, was, in general, found to be the result of a cooperative effect. The catalytic systems comprise diverse solvents and reaction conditions while using the Lewis and Brønsted acid properties of the catalysts. More importantly, because of the presence of Lewis and Brønsted acid sites, MOFs are also known to be good catalysts for epoxide ring-opening reactions in the presence of nucleophiles such as amines, alcohols, and azides.<sup>14,21,49–58</sup> In particular, MOFs with a potential to generate CUSs are known to be active Lewis acid catalysts for ERO reactions.<sup>52,57</sup> On the other hand, example of MOFs with Brønsted acid sites acting as catalysts for methanolysis of epoxides are also available.<sup>21,50</sup> Therefore, ERO reactions will provide an opportunity to test our hypothesis: (i) Metal centers with coordinated DMF can act as Lewis acid sites through facile exchange of DMF with epoxide. (ii) The subsequent attack of amine (aminolysis) will lead to a chemo- and/or stereoselective product based on the pore structure and nature of the SBU. Accordingly, the reaction of propylene oxide (3 mmol) and *N*-methylaniline (1 mmol) using MST-2(Co–Zn) (30 mg) at 25 °C in neat conditions selectively gave 1-[methyl(phenyl-amino)]propan-2-ol in 20% yield (Table S1, entry 1). The reaction occurred chemoselectively at the less hindered site of terminal epoxide, giving type II alcohol (see the Supporting Information, section 1.2). Tuning the temperature from 25 to 40 °C increased the yield to 42% (Table S1, entry 2), whereas changing the catalyst loading to 50 mg (~5 mol %) produced 89%  $\beta$ -hydroxyamine (Table 2, entry 2) in 14 h, as shown in

**Table 2.** Co–Zn MOFs Catalyzed Ring-Opening Reaction of Propylene Oxide with *N*-Methylaniline<sup>a</sup>



entry	catalyst	yield (%) <sup>b</sup>
1	MST-1(Co–Zn)	84
2	MST-2(Co–Zn)	89
3	MST-1(Zn)	87
4	MST-2(Zn)	90
5	none	<5

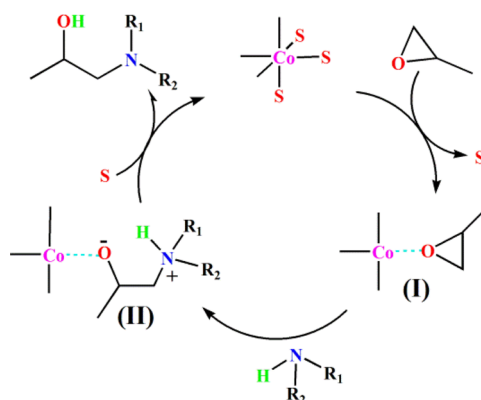
<sup>a</sup>Optimized reaction conditions: catalyst (50 mg), *N*-methylaniline (1 mmol), propylene oxide (3 mmol), molecular sieves (5 Å, 30 mg), neat; stirred for 14 h at 40 °C. <sup>b</sup>Yield determined by <sup>1</sup>H NMR.

the time–conversion plot (Figure S14). An identical reaction using MST-1(Co–Zn) (50 mg) as the catalyst at 25 °C selectively yielded 55%  $\beta$ -hydroxyamine (Table S1, entry 4) and 84% at 40 °C (Table 2, entry 1). As a control, reactions without any catalyst under identical conditions gave negligible products (Table 2, entry 5), showing the role of MOFs in the catalytic process. Reaction using the pure zinc phases of the MOFs MST-1(Zn) and MST-2(Zn) gave identical reactivity with absolute chemoselectivity (Table 2, entries 3 and 4), generalizing the influence of the 3D frameworks in directing the reaction to a fixed pathway. The activation of epoxide on the metal center was further substantiated through the reaction of other secondary amines with varying basicity and steric environment. The reaction of propylene oxide with aliphatic amines such as morpholine ( $pK_a = 8.36$ ), diethylamine ( $pK_a = 10.98$ ), and piperidine ( $pK_a = 11.22$ ) gave almost quantitative

conversions (<98%; Table S2, entries 1–8). However, reaction with sterically crowded amines such as diisopropylamine ( $pK_a = 11.05$ ) and *N,N'*-diphenylamine ( $pK_a = 0.80$ ) produced conversion of less than 5% and can be rightly correlated to steric congestion. The influence of steric congestion on the overall yield strongly indicates a situation where the reaction is taking place on the metal center inside the pores via the activation of epoxide. This further excludes the role of any Brønsted acid, which otherwise would not have any effect over the catalytic output and exemplifies the involvement of a metal Lewis acid center. The loss of catalytic reactivity upon reaction in an organic solvent further supports the competition of solvent molecules with epoxides for the active site, resulting in activity loss (Table S1, entries 6–8).

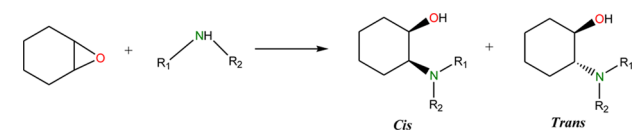
**Mechanistic Consideration.** On the basis of the reactivity and product profiles, a simplified plausible mechanism (Scheme 2) for the catalytic process is proposed. The reaction gets

**Scheme 2.** Plausible Reaction Mechanism for the Catalytic ERO Reaction



initiated by the activation of epoxide onto the metal center (I), which brings rigidity and directs the nucleophilic addition of amines toward the least hindered C center (II), chemo-selectively giving rise to secondary  $\beta$ -hydroxyamine. The almost negligible yield of sterically demanding amines further shows the hindered accessibility of the substrate in the crystalline framework and excludes the participation of external surface sites in the catalysis. Although surface areas are low, epoxides can still exchange with the coordinated DMF and small amines can diffuse into the framework. A similar low surface area observed in a bimetallic 3D network with well-defined pores and yet showing ERO catalysis due to active sites inside the pores was reported previously by Kumar and Gupta.<sup>57</sup> Repetitive recycling of MST-1/MST-2 shows fairly good activity with more than 70% conversion for the fifth cycle (Figure S15). No noticeable sign of structural changes is visible in the PXRD measurements of the recycled catalyst until the third cycle (Figure S16); however, unambiguous characterization of structural modifications in the SBUs needs more detailed study. Furthermore, the addition of amine and epoxide onto the supernatant liquid from the washings gave no amination reactions, confirming the heterogeneity of the catalytic system. The difference in the reactivity between MST-1 and MST-2 was quite distinct in the catalytic ring-opening reaction of symmetric cyclohexene oxide with amine (Table 3). MST-2 diastereoselectively gave the *trans*- $\beta$ -hydroxyamine exclusively with all of the secondary amines (Table 3, entries 1, 3, 5, and 7) under study, whereas MST-1

**Table 3. Catalytic Ring-Opening Reaction of Cyclohexene Oxide with Secondary Amines<sup>a</sup>**



Entry	Amine	Catalyst	Conversion	Selectivity (%) <sup>b</sup>
1		MST-2 (Co-Zn)	97%	trans - 100%
2		MST-1 (Co-Zn)	85%	trans - 88%
3		MST-2 (Co-Zn)	98%	trans-100%
4		MST-1 (Co-Zn)	95%	trans - 55%
5		MST-2 (Co-Zn)	99%	trans-100%
6		MST-1 (Co-Zn)	98%	trans - 35%
7		MST-2 (Co-Zn)	65%	trans-100%
8		MST-1 (Co-Zn)	35%	trans-70%

<sup>a</sup>Reaction condition: catalyst (50 mg), amines (1 mmol), cyclohexene oxide (1 mmol), molecular sieves (5 Å, 30 mg); neat; stirred for 12 h at 40 °C. <sup>b</sup>Yield determined by <sup>1</sup>H NMR.

yielded a mixture of both *cis*- and *trans*-alcohol (Table 3, entries 2, 4, 6, and 8, and see the Supporting Information, section 1.3). This proves that, besides the presence of Lewis acidic metal sites, the structures of the pores and disposition of the Lewis acidic sites in the channel are important factors in determining the stereoselective product formation. Attempts to collect single-crystal data on ex situ treated MST-1/MST-2 with amines and/or epoxide to trap the activated complex turned futile because of the loss of single crystallinity. Nevertheless, considering the reaction to be exclusively heterogeneous, preliminary catalytic results clearly show strong differences of their selectivity based on the crystal system and subtle differences in the SBUs.

## CONCLUSIONS

In summary, we reported hexagonal and tetragonal, mono-metallic Zn and bimetallic Co/Zn MOFs based on BTC<sup>3-</sup> that evolved as excellent frameworks to study the structure activity relationship in MOFs. The phases chemoselectively catalyze the epoxide ring-opening reaction heterogeneously and show marked differences in the diastereoselectivity. This work presents an exclusive example of structure-dependent catalytic activity in MOFs, and further work to generalize the catalytic process is currently underway.

## ASSOCIATED CONTENT

### Supporting Information

The Supporting Information is available free of charge on the ACS Publications website at DOI: 10.1021/acs.inorgchem.6b01288.

Experimental procedures, PXRD patterns, FT-IR, NMR, TGA, magnetic susceptibility plots, and surface area measurements (PDF)  
X-ray crystallographic data in CIF format for MST-1(Co-Zn), MST-2(Co-Zn), and MST-2(Zn) (CIF)

## AUTHOR INFORMATION

### Corresponding Author

\*E-mail: choudhurya@mst.edu.

### Present Address

<sup>‡</sup>A.P.: Department of Chemistry, Sikkim University, Gangtok 737102, Sikkim, India.

### Notes

The authors declare no competing financial interest.

## ACKNOWLEDGMENTS

The authors acknowledge funding from the ERDC (Missouri University of Science and Technology) and University of Missouri Research Board. The authors also acknowledge Dr. Ghosh, Missouri State University, Springfield, MO, and Dr. Liang, Missouri University of Science and Technology, Rolla, MO, for their help with the magnetic and surface area measurements, respectively.

## REFERENCES

- Ockwig, N. W.; Delgado-Friedrichs, O.; O'Keeffe, M.; Yaghi, O. M. Reticular Chemistry: Occurrence and Taxonomy of Nets and Grammar for the Design of Frameworks. *Acc. Chem. Res.* **2005**, *38*, 176–182.
- Férey, G. Hybrid porous solids: past, present, future. *Chem. Soc. Rev.* **2008**, *37*, 191–214.
- Férey, G.; Serre, C. Large breathing effects in three-dimensional porous hybrid matter: facts, analyses, rules and consequences. *Chem. Soc. Rev.* **2009**, *38*, 1380–1399.
- Furukawa, H.; Cordova, K. E.; O'Keeffe, M.; Yaghi, O. M. The chemistry and applications of metal-organic frameworks. *Science* **2013**, *341*, 1230444.
- Yaghi, O. M.; O'Keeffe, M.; Ockwig, N. W.; Chae, H. K.; Eddaoudi, M.; Kim, J. Reticular synthesis and the design of new materials. *Nature* **2003**, *423*, 705–714.
- Stavitski, E.; Goesten, M.; Juan-Alcañiz, J.; Martinez-Joaristi, A.; Serra-Crespo, P.; Petukhov, A. V.; Gascon, J.; Kapteijn, F. Kinetic Control of Metal–Organic Framework Crystallization Investigated by Time-Resolved In Situ X-Ray Scattering. *Angew. Chem., Int. Ed.* **2011**, *50*, 9624–9628.
- Millange, F.; Medina, M.; Guillou, N.; Férey, G.; Golden, K. M.; Walton, R. I. Time-Resolved In Situ Diffraction Study of the Solvothermal Crystallization of Some Prototypical Metal–Organic Frameworks. *Angew. Chem., Int. Ed.* **2010**, *49*, 763–766.
- Millange, F.; El Osta, R.; Medina, M. E.; Walton, R. I. A time-resolved diffraction study of a window of stability in the synthesis of a copper carboxylate metal–organic framework. *CrystEngComm* **2011**, *13*, 103–108.
- O'Keeffe, M.; Yaghi, O. M. Deconstructing the Crystal Structures of Metal–Organic Frameworks and Related Materials into Their Underlying Nets. *Chem. Rev.* **2012**, *112*, 675–702.
- Sumida, K.; Rogow, D. L.; Mason, J. A.; McDonald, T. M.; Bloch, E. D.; Herm, Z. R.; Bae, T.-H.; Long, J. R. Carbon Dioxide Capture in Metal–Organic Frameworks. *Chem. Rev.* **2012**, *112*, 724–781.
- Rosi, N. L.; Eckert, J.; Eddaoudi, M.; Vodak, D. T.; Kim, J.; O'Keeffe, M.; Yaghi, O. M. Hydrogen storage in microporous metal-organic frameworks. *Science* **2003**, *300*, 1127–1129.
- Corma, A.; García, H.; Llabrés i Xamena, F. X. Engineering Metal Organic Frameworks for Heterogeneous Catalysis. *Chem. Rev.* **2010**, *110*, 4606–4655.
- Gascon, J.; Corma, A.; Kapteijn, F.; Llabrés i Xamena, F. X. Metal Organic Framework Catalysis: Quo vadis? *ACS Catal.* **2014**, *4*, 361–378.
- Krap, C. P.; Newby, R.; Dhakshinamoorthy, A.; García, H.; Cebula, I.; Eason, T. L.; Savage, M.; Eyley, J. E.; Gao, S.; Blake, A. J.; Lewis, W.; Beton, P. H.; Warren, M. R.; Allan, D. R.; Frogley, M. D.;



- Tang, C. C.; Cinque, G.; Yang, S.; Schroder, M. Enhancement of CO<sub>2</sub> Adsorption and Catalytic Properties by Fe-Doping of [Ga<sub>2</sub>(OH)<sub>2</sub>(L)] (H<sub>2</sub>L = Biphenyl-3,3',5,5'-tetracarboxylic Acid), MFM-300(Ga<sub>2</sub>). *Inorg. Chem.* **2016**, *55*, 1076–1088.
- (15) Dhakshinamoorthy, A.; Asiri, A. M.; Garcia, H. Mixed-metal or mixed-linker metal organic frameworks as heterogeneous catalysts. *Catal. Sci. Technol.* **2016**, *6*, 5238–5261.
- (16) Ma, L.; Abney, C.; Lin, W. Enantioselective catalysis with homochiral metal-organic frameworks. *Chem. Soc. Rev.* **2009**, *38*, 1248–1256.
- (17) Lee, J.; Farha, O. K.; Roberts, J.; Scheidt, K. A.; Nguyen, S. T.; Hupp, J. T. Metal-organic framework materials as catalysts. *Chem. Soc. Rev.* **2009**, *38*, 1450–1459.
- (18) Feng, D.; Chung, W. C.; Wei, Z.; Gu, Z. Y.; Jiang, H. L.; Chen, Y. P.; Darensbourg, D. J.; Zhou, H. C. Construction of Ultrastable Porphyrin Zr Metal-Organic Frameworks through Linker Elimination. *J. Am. Chem. Soc.* **2013**, *135*, 17105–17110.
- (19) Zhang, M.; Bosch, M.; Gentle, T., III; Zhou, H. C. Rational design of metal-organic frameworks with anticipated porosities and functionalities. *CrystEngComm* **2014**, *16*, 4069–4083.
- (20) Tanabe, K. K.; Cohen, S. M. Modular, Active, and Robust Lewis Acid Catalysts Supported on a Metal-Organic Framework. *Inorg. Chem.* **2010**, *49*, 6766–6774.
- (21) Garibay, S. J.; Wang, Z.; Cohen, S. M. Evaluation of Heterogeneous Metal-Organic Framework Organocatalysts Prepared by Postsynthetic Modification. *Inorg. Chem.* **2010**, *49*, 8086–8091.
- (22) Ma, L.; Wu, C. D.; Wanderley, M. M.; Lin, W. Single-Crystal to Single-Crystal Cross-Linking of an Interpenetrating Chiral Metal-Organic Framework and Implications in Asymmetric Catalysis. *Angew. Chem., Int. Ed.* **2010**, *49*, 8244–8248.
- (23) Ma, L.; Falkowski, J. M.; Abney, C.; Lin, W. A series of isorecticular chiral metal-organic frameworks as a tunable platform for asymmetric catalysis. *Nat. Chem.* **2010**, *2*, 838–846.
- (24) Cohen, S. M. Postsynthetic Methods for the Functionalization of Metal-Organic Frameworks. *Chem. Rev.* **2012**, *112*, 970–1000.
- (25) Wu, C.-D.; Lin, W. Heterogeneous Asymmetric Catalysis with Homochiral Metal-Organic Frameworks: Network-Structure-Dependent Catalytic Activity. *Angew. Chem., Int. Ed.* **2007**, *46*, 1075–1078.
- (26) Kubelka, P.; Munk, F. Z. Ein Beitrag zur Optik der Farbanstriche. *Technol. Phys.* **1931**, *12*, 593–601.
- (27) SMART; Bruker AXS Inc.: Madison, WI, 2002.
- (28) SAINT; Bruker AXS Inc.: Madison, WI, 2008. SADABS; Bruker AXS Inc.: Madison, WI, 2008.
- (29) Sheldrick, G. M. A short history of SHELX. *Acta Crystallogr., Sect. A: Found. Crystallogr.* **2008**, *64*, 112–122.
- (30) Kim, J.; Chen, B.; Reineke, T. M.; Li, H.; Eddaoudi, M.; Moler, D. B.; O'Keeffe, D. B.; Yaghi, O. M. Assembly of Metal-Organic Frameworks from Large Organic and Inorganic Secondary Building Units: New Examples and Simplifying Principles for Complex Structures. *J. Am. Chem. Soc.* **2001**, *123*, 8239–8247.
- (31) Gao, J.; Ye, K.; Yang, L.; Xiong, W.-W.; Ye, L.; Wang, Y.; Zhang, Q. Growing Crystalline Zinc-1,3,5-benzenetricarboxylate Metal-Organic Frameworks in Different Surfactants. *Inorg. Chem.* **2014**, *53*, 691–693.
- (32) He, J.; Zhang, Y.; Pan, Q.; Yu, J.; Ding, H.; Xu, R. Three metal-organic frameworks prepared from mixed solvents of DMF and HAc. *Microporous Mesoporous Mater.* **2006**, *90*, 145–152.
- (33) Caskey, S. R.; Matzger, A. J. Selective Metal Substitution for the Preparation of Heterobimetallic Microporous Coordination Polymers. *Inorg. Chem.* **2008**, *47*, 7942–7944.
- (34) Ma, R.; Liu, Z.; Takada, K.; Fukuda, K.; Ebina, Y.; Bando, Y.; Sasaki, T. Tetrahedral Co(II) Coordination in  $\alpha$ -Type Cobalt Hydroxide: Rietveld Refinement and X-ray Absorption Spectroscopy. *Inorg. Chem.* **2006**, *45*, 3964–3969.
- (35) Taylor, J. M.; Thompson, R. C. Magnetic and Spectral Studies on Cobalt(II) Fluorosulfate. *Can. J. Chem.* **1971**, *49*, 511–515.
- (36) Ager, D. J.; Prakash, I.; Schaad, D. R. 1,2-Amino Alcohols and Their Heterocyclic Derivatives as Chiral Auxiliaries in Asymmetric Synthesis. *Chem. Rev.* **1996**, *96*, 835–876.
- (37) Jacobsen, E. N. Asymmetric Catalysis of Epoxide Ring-Opening Reactions. *Acc. Chem. Res.* **2000**, *33*, 421–431.
- (38) Chakraborti, A. K.; Rudrawar, S.; Kondaskar, A. An efficient synthesis of 2-amino alcohols by silica gel catalysed opening of epoxide rings by amines. *Org. Biomol. Chem.* **2004**, *2*, 1277–1280.
- (39) Posner, G. H.; Rogers, D. Z. Organic reactions at alumina surfaces. Mild and selective opening of epoxides by alcohols, thiols, benzeneselenol, amines, and acetic acid. *J. Am. Chem. Soc.* **1977**, *99*, 8208–8214.
- (40) Chini, M.; Crotti, P.; Macchia, F. Metal salts as new catalysts for mild and efficient aminolysis of oxiranes. *Tetrahedron Lett.* **1990**, *31*, 4661–4664.
- (41) Sekar, S.; Singh, V. K. An Efficient Method for Cleavage of Epoxides with Aromatic Amines. *J. Org. Chem.* **1999**, *64*, 287–289.
- (42) Auge, J.; Leroy, F. Lithium trifluoromethanesulfonate-catalysed aminolysis of oxiranes. *Tetrahedron Lett.* **1996**, *37*, 7715–7716.
- (43) Curini, M.; Epifano, F.; Marcotullio, M. C.; Rosati, O. Zirconium Sulfophenyl Phosphonate as a Heterogeneous Catalyst in the Preparation of  $\beta$ -Amino Alcohols from Epoxides. *Eur. J. Org. Chem.* **2001**, *21*, 4149–4152.
- (44) Chakraborti, A. K.; Kondaskar, A. ZrCl<sub>4</sub> as a new and efficient catalyst for the opening of epoxide rings by amines. *Tetrahedron Lett.* **2003**, *44*, 8315–8319.
- (45) Iqbal, J.; Pandey, A. An unusual chemoselectivity in cobalt(II) chloride catalysed cleavage of oxiranes with anilines: A highly regioselective synthesis of  $\beta$ -amino alcohols. *Tetrahedron Lett.* **1990**, *31*, 575–576.
- (46) Durán Pachón, L.; Gamez, P.; Van Brussel, J. J. M.; Reedijk, J. Zinc-catalysed aminolysis of epoxides. *Tetrahedron Lett.* **2003**, *44*, 6025–6027.
- (47) Sabitha, G.; Kumar Reddy, G. S.; Bhaskar Reddy, K.; Yadav, J. S. Vanadium(III) Chloride-Catalyzed Preparation of  $\beta$ -Amino Alcohols from Epoxides. *Synthesis* **2003**, 2298–2300.
- (48) Roy, S. R.; Nijamudheen, A.; Pariyar, A.; Ghosh, A.; Vardhanapu, P. K.; Mandal, P. K.; Datta, A.; Mandal, S. K. Phenalenyl in a Different Role: Catalytic Activation through the Nonbonding Molecular Orbital. *ACS Catal.* **2014**, *4*, 4307–4319.
- (49) Tanaka, K.; Oda, S.; Shiro, M. A novel chiral porous metal-organic framework: asymmetric ring opening reaction of epoxide with amine in the chiral open space. *Chem. Commun.* **2008**, 820–822.
- (50) Ingleson, M. J.; Barrio, J. P.; Bacsá, J.; Dickinson, C.; Park, H.; Rosseinsky, M. Generation of a solid Brønsted acid site in a chiral framework. *Chem. Commun.* **2008**, 1287–1289.
- (51) Jiang, D.; Mallat, T.; Krumeich, F.; Baiker, A. Copper-based metal-organic framework for the facile ring-opening of epoxides. *J. Catal.* **2008**, *257*, 390–395.
- (52) Dhakshinamoorthy, A.; Alvaro, M.; Garcia, H. Metal-Organic Frameworks as Efficient Heterogeneous Catalysts for the Regioselective Ring Opening of Epoxides. *Chem. - Eur. J.* **2010**, *16*, 8530–8536.
- (53) Kumar, G.; Singh, A. P.; Gupta, R. Synthesis, Structures, and Heterogeneous Catalytic Applications of {Co<sup>3+</sup>-Eu<sup>3+</sup>} and {Co<sup>3+</sup>-Tb<sup>3+</sup>} Heterodimetallic Coordination Polymers. *Eur. J. Inorg. Chem.* **2010**, *2010*, 5103–5112.
- (54) Biswas, S.; Maes, M.; Dhakshinamoorthy, A.; Feyand, M.; De Vos, D. E.; Garcia, H.; Stock, N. Fuel purification, Lewis acid and aerobic oxidation catalysis performed by a microporous Co-BTT (BTT<sup>3-</sup> = 1,3,5-benzenetris-tetrazolate) framework having coordinatively unsaturated sites. *J. Mater. Chem.* **2012**, *22*, 10200–10209.
- (55) Tanaka, K.; Otani, K.-I.; Murase, T.; Nishihote, S.; Urbanczyk-Lipkowska, Z. Enantioselective Ring-Opening Reaction of Epoxides with MeOH Catalyzed by Homochiral Metal-Organic Framework. *Bull. Chem. Soc. Jpn.* **2012**, *85*, 709–714.
- (56) Dhakshinamoorthy, A.; Alvaro, M.; Garcia, H. Commercial metal-organic frameworks as heterogeneous catalysts. *Chem. Commun.* **2012**, *48*, 11275–11288.

(57) Kumar, G.; Gupta, R. Three-Dimensional  $\{\text{Co}^{3+}\text{-Zn}^{2+}\}$  and  $\{\text{Co}^{3+}\text{-Cd}^{2+}\}$  Networks Originated from Carboxylate-rich Building Blocks: Syntheses, Structures, and Heterogeneous Catalysis. *Inorg. Chem.* **2013**, *52*, 10773–10787.

(58) García-García, P.; Müller, M.; Corma, A. MOF catalysis in relation to their homogeneous counterparts and conventional solid catalysts. *Chem. Sci.* **2014**, *5*, 2979–3007.